



OPEN ACCESS

EDITED BY

Ping Xiang,
Central South University, China

REVIEWED BY

Han Zhao,
City University of Hong Kong, Hong
Kong SAR, China
Chuanqing Fu,
Zhejiang University of Technology, China

*CORRESPONDENCE

Jinrui Zhang,
✉ 335257@whut.edu.cn

RECEIVED 14 August 2024

ACCEPTED 23 September 2024

PUBLISHED 07 October 2024

CITATION

Li J, Li F, Mao M, Zhang J and Fan R (2024)
Characteristics of dynamic mechanics and
energy loss in reef limestone concrete during
dry-wet carbonation periods.
Front. Mater. 11:1480674.
doi: 10.3389/fmats.2024.1480674

COPYRIGHT

© 2024 Li, Li, Mao, Zhang and Fan. This is an
open-access article distributed under the
terms of the [Creative Commons Attribution
License \(CC BY\)](https://creativecommons.org/licenses/by/4.0/). The use, distribution or
reproduction in other forums is permitted,
provided the original author(s) and the
copyright owner(s) are credited and that the
original publication in this journal is cited, in
accordance with accepted academic practice.
No use, distribution or reproduction is
permitted which does not comply with
these terms.

Characteristics of dynamic mechanics and energy loss in reef limestone concrete during dry-wet carbonation periods

Jian Li¹, Fei Li², Mingju Mao³, Jinrui Zhang^{3*} and Ran Fan³

¹Department of Architecture Engineering and Design, Wuhan Institute of Shipbuilding Technology, Wuhan, China, ²Department of Road and Bridge Engineering, Guizhou Communications Polytechnic University, Guiyang, China, ³Wuhan University of Technology, Wuhan, China

Coral reef limestone is a unique type of rock and soil body characterized by high porosity. Its dynamic mechanical properties under impact loads differ significantly from those of conventional land-sourced aggregate concrete. This study utilizes coral reef limestone as both coarse and fine aggregates to prepare C40 strength concrete. The research investigates the effects of dry-wet carbonation cycles on its dynamic mechanical behavior and energy evolution characteristics using a Split Hopkinson Pressure Bar (SHPB) mechanical testing system. The findings reveal that increasing the number of dry-wet carbonation cycles leads to a significant weakening of the internal structural bonding in coral reef limestone concrete. Notably, the degree of phenolphthalein color change diminishes, while uniaxial compressive strength and tensile strength demonstrate an overall downward trend. The reduction in tensile strength is less pronounced than the decrease in compressive strength. Additionally, the relative dynamic elastic modulus gradually decreases, and a size effect is noted, with a rapid acceleration in mass loss. As the number of dry-wet carbonation cycles increases, dynamic compressive strength declines, and failure modes shift from surface cracking to crush-type failure. The dynamic increase factor (DIF) of the coral reef limestone concrete indicates a high sensitivity to strain rate, with a significant rise in DIF value as the strain rate increases. Various energies generated under impact load exhibit clear strain rate effects. Furthermore, the effects of dry-wet carbonation cycling enhance energy dissipation, especially at 30 cycles, where energy dissipation increases sharply, while a hindering effect on transmitted energy is observed.

KEYWORDS

reef limestone concrete, dry-wet carbonation cycle, dynamic fragmentation, strain rate, energy dissipation

1 Introduction

The engineering projects on the coral reefs in Western Pacific Ocean waters are far from the mainland, leading to a severe scarcity of mainland-sourced mechanized sand aggregates and freshwater resources. Transporting sand, gravel, and other concrete materials from the mainland not only increases construction costs but also impacts the construction schedule. Utilizing local materials by preparing concrete from reef limestone for the construction of island reef projects alleviates the issue of raw material shortages

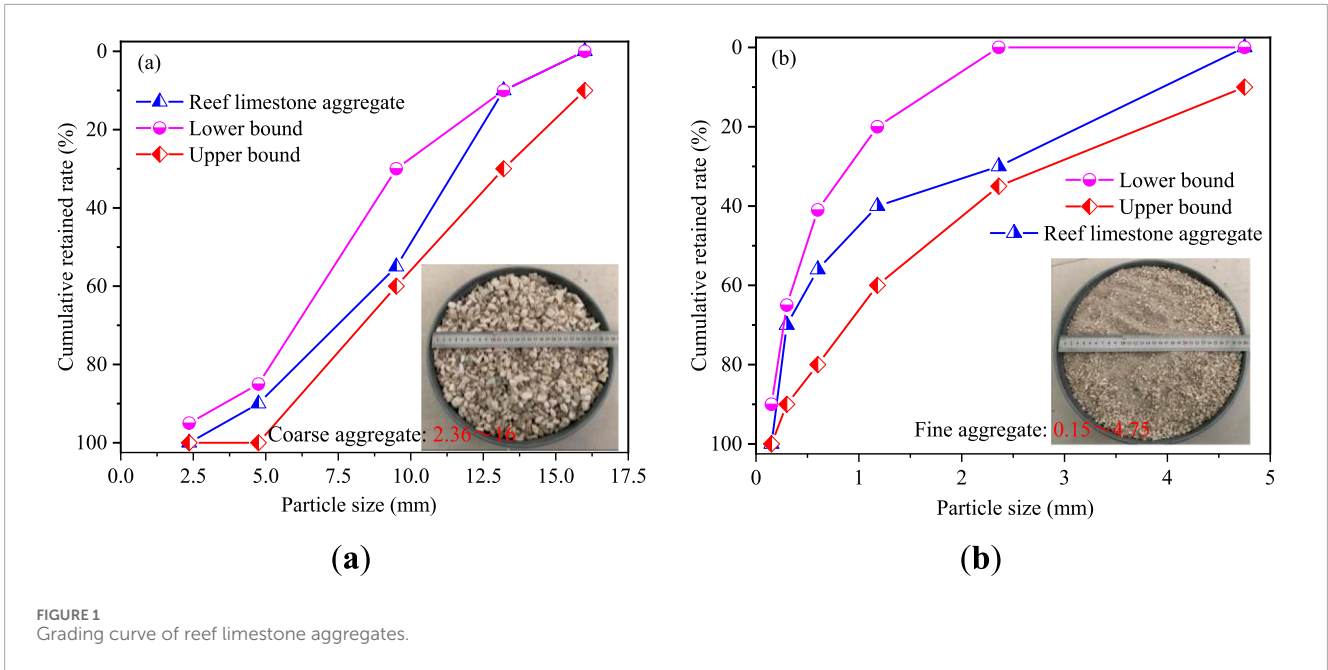
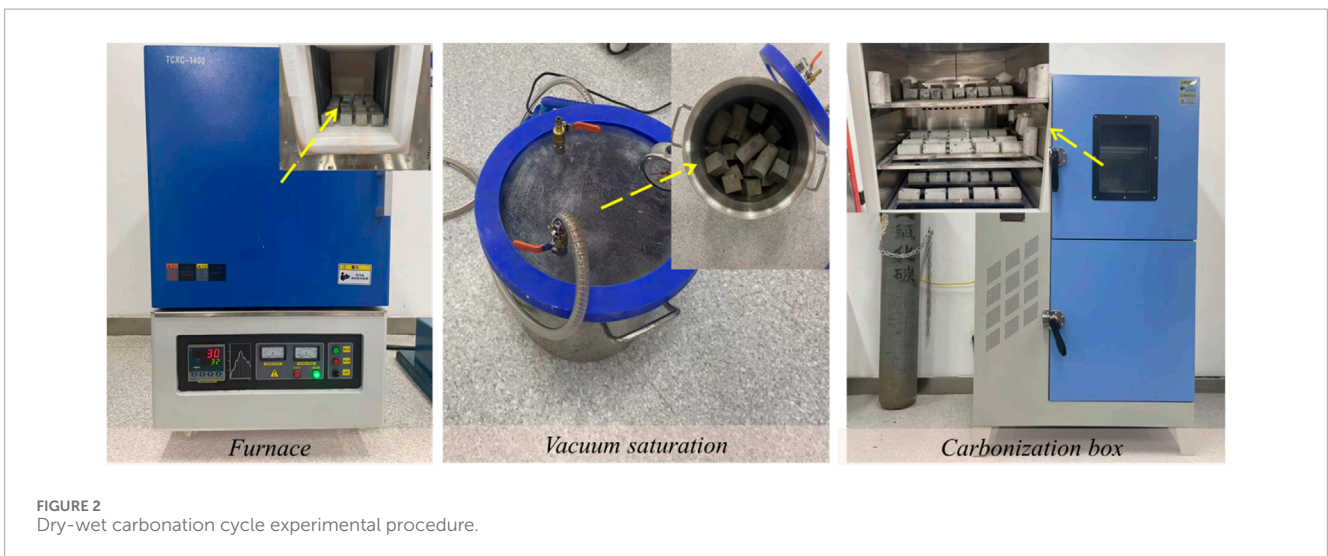


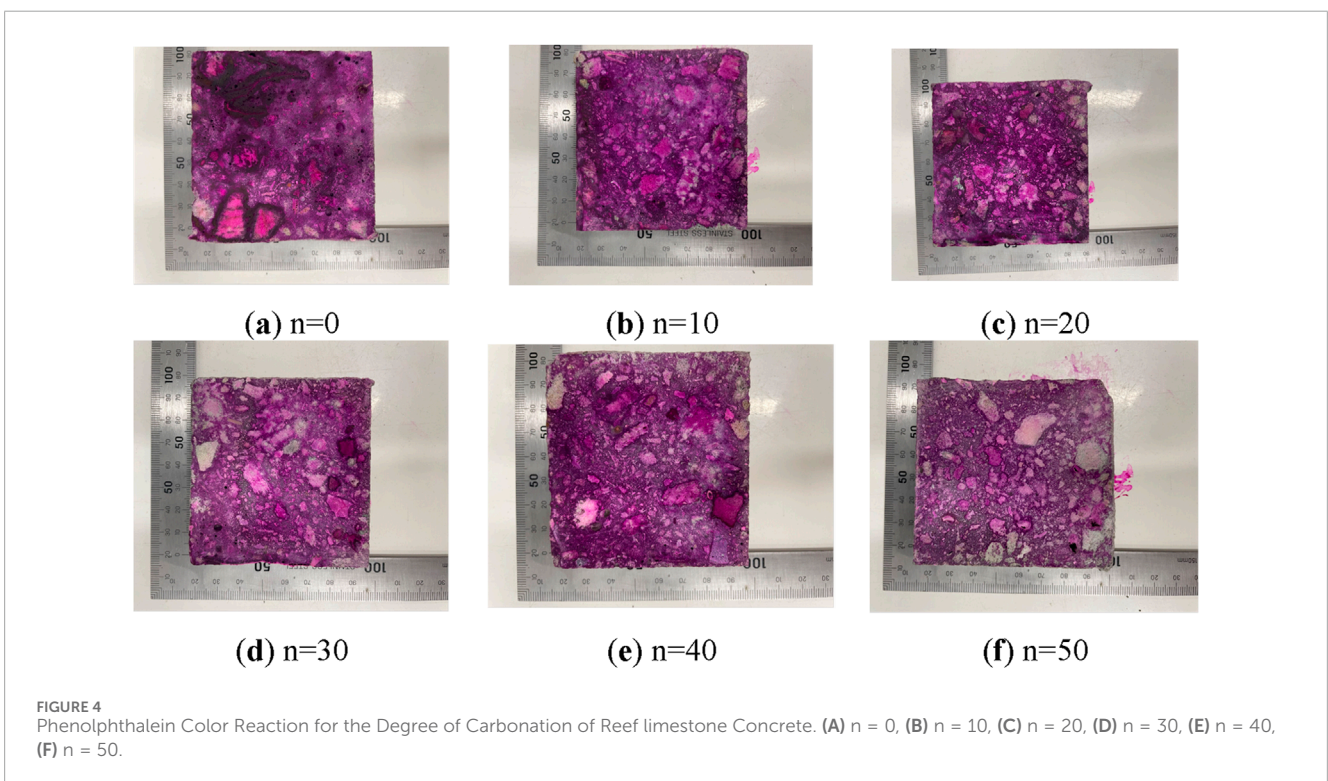
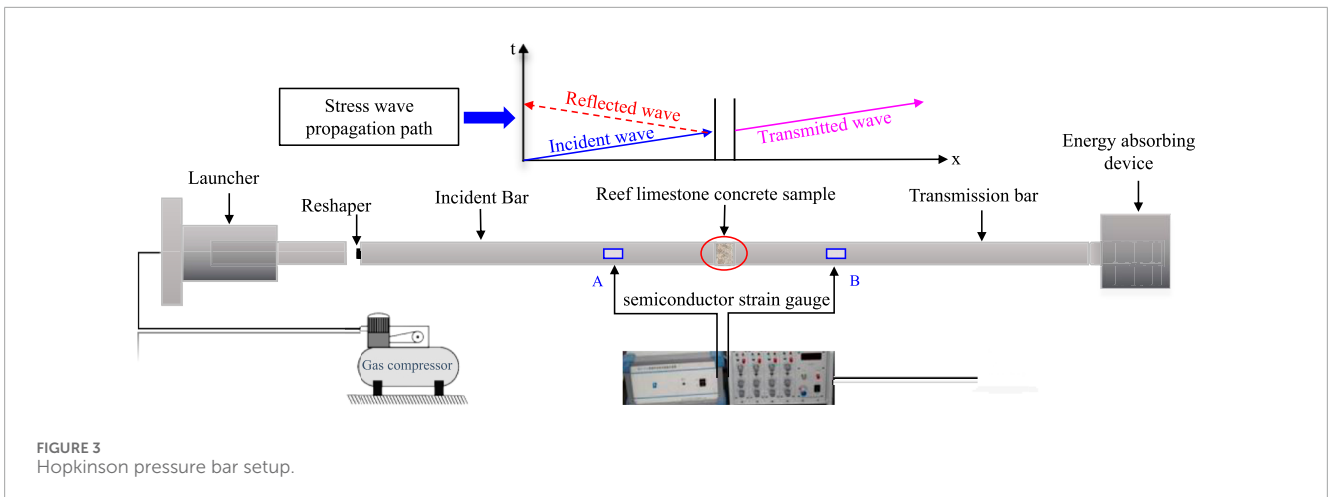
TABLE 1 Mix proportions of reef limestone concrete (kg/m³).

Name	Ordinary portland cement	Reef limestone	Reef limestone	Seawater	Fly ash	Slag	Crack-resistant waterproofing agent
Amount	780	700	300	250	70	150	15



in marine engineering and allows for the reasonable development and use of marine resources according to local conditions (Deng et al., 2022; Zhou et al., 2020). Furthermore, the structural designs of coral reefs in Western Pacific Ocean waters are designed to endure not just static forces but also diverse dynamic forces, including earthquakes, tsunamis, and unintended blasts. This places strict requirements on the selection and design

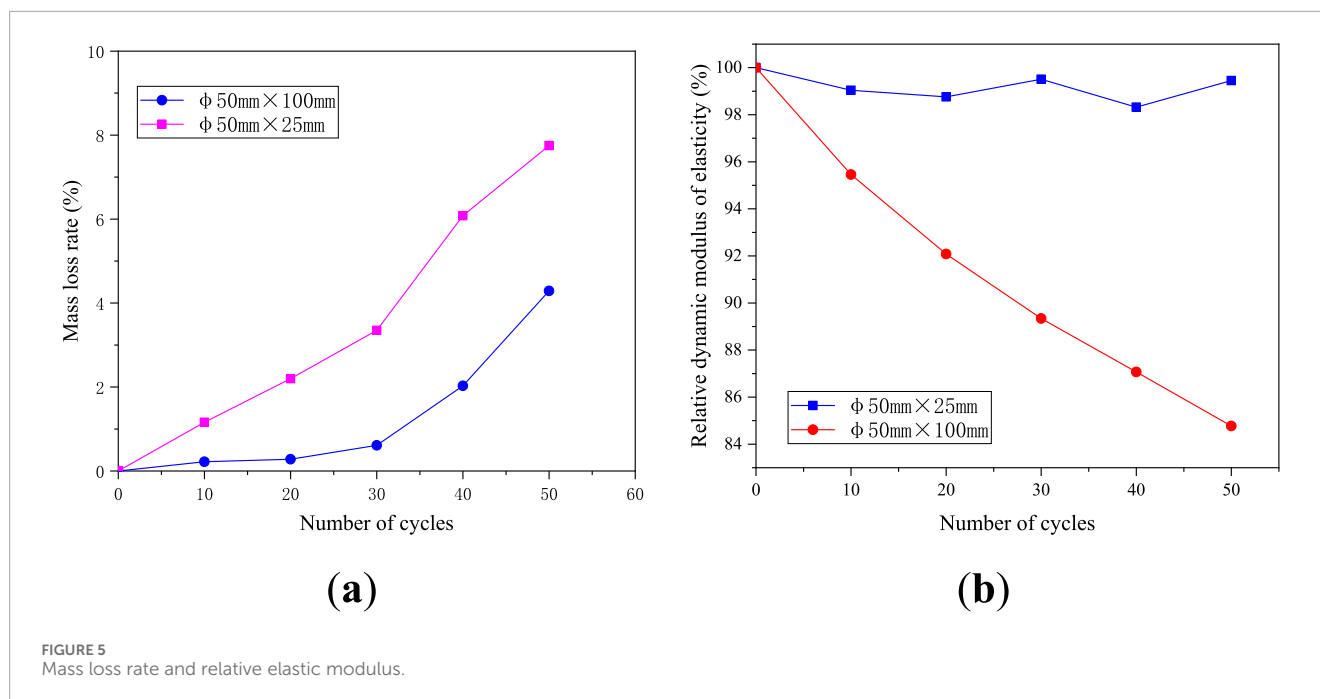
of building materials for their impact resistance (Lahiri et al., 2022). At the same time, the structures on the reefs inevitably face the harsh service environment affected by long-term dry-wet carbonation cycles (Liu et al., 2023), This leads to the deterioration of concrete structural performance and a reduction in service life, which severely threatens the long-term stability of reef projects. Consequently, researching the dynamic mechanical efficiency of



reef limestone concrete in response to dry-wet carbonation cycles is crucial.

As a unique geomaterial, coral reef limestone is extensively found across Western Pacific Ocean waters (Zhang et al., 2023). In the 1940s, some marine infrastructure construction projects began to involve coral reef limestone concrete (Fu et al., 2021). Concrete, a tripartite medium made up of aggregates, the interface transition zone, and cement paste, plays a significant role in determining its performance (Meddah et al., 2010; Uddin et al., 2017). Research indicates that fissures in light aggregate concrete mainly infiltrate the aggregates, in contrast to traditional aggregate concrete where cracks predominantly emerge at the junction of the aggregates and the paste (Sim et al., 2013), Reef limestone aggregates fall into the category of typical lightweight aggregates, and the surfaces of reef

limestone coarse aggregates are porous and rough. Consequently, the way reef limestone concrete fails when subjected to external loads is markedly distinct compared to other light aggregates and standard concrete. Wu et al. (2020) discovered that reef limestone concrete's dynamic compressive strength, when subjected to impact loads, surpasses that of standard concrete of identical quality, yet falls marginally short of other light aggregate concretes. Wu et al. (2019); Ma et al. (2020) discovered that reef limestone aggregate concrete, maintaining identical strength and minimal strain rates, shows reduced static and dynamic compressive strengths compared to traditional aggregate concrete, yet its dynamic increase factor (DIF) demonstrates a more pronounced strain rate impact. It was found that the primary formation of cracks in reef limestone concrete occurs via the aggregates of reef limestone, rather than at the



junction of these aggregates and the paste (Ma et al., 2019). Qin et al. (2023) examined the evolving properties, patterns of energy development, modes of fractures, and damage processes in coral reef sand concrete when subjected to impact forces.

Concrete structures inevitably face various harsh environmental challenges during their service life, including extreme weather changes, chemical corrosion, water infiltration, and physical impacts. Mumenya et al. (2010) found that concrete materials exposed to specific environments, such as dry-wet cycles, for extended periods experience certain changes in mechanical properties. Donnini (2019) investigated the mechanical characteristics of two varieties of concrete in solutions varying in temperature and pH, discovering that the mechanical attributes of standard concrete show minimal sensitivity to changes in temperature and pH; however, there is a notable impact on the tensile strength of glass fiber concrete. Li et al. (2021); Yin et al. (2019) studied to understand the deterioration trends of mechanical properties in recycled concrete under freeze-thaw cycles in both salt solutions and dry-wet conditions. Zhang et al. (2024) used waste glass instead of sand as fine aggregate to study the performance change of concrete after dry-wet cycle. Xu et al. (2021) investigated the combined impact of hybrid fibers on concrete's longevity and additionally forecasted the durability of fiber-reinforced concrete under carbonation and chloride ion corrosion conditions.

The evaluation of reef limestone concrete's bearing capacity and durability, a novel deep-sea island reef construction material, is still in its initial stages of exploration and verification, facing notable limitations in its adaptability studies in severe marine conditions. Coral reef limestone aggregates are naturally characterized by their loose and porous properties, making them highly susceptible to corrosion from marine gaseous environments. Previous studies have focused more on the static mechanical properties of coral reef limestone concrete in harsh marine environments, while research on its durability under dynamic impact loads has

been insufficient. Consequently, this research utilizes a divided Hopkinson pressure bar for performing impact assessments on reef limestone concrete samples undergoing dry-wet carbonation processes. This study explores how dry-wet carbonation cycles impact the dynamic compressive strength, modes of failure, and energy development traits of reef limestone concrete, and delves into the inherent connections among loading speeds, fracturing traits, and energy loss properties when dry-wet carbonation is combined. The results offer theoretical backing for the creation and advancement of novel concrete frameworks in the field of island reef engineering.

2 Materials and methods

2.1 Preparation of reef limestone concrete samples

Limestone samples from a reef on an island in Western Pacific Ocean waters were synthetically pulverized into particles, each not exceeding 16 mm in size. Particles measuring 4.75–16 mm in size were processed as coarse aggregate, whereas those ranging from 0.15 to 4.75 mm were selected for fine aggregate (Fan et al., 2023; Liu et al., 2018). Figure 1 elaborates on the ongoing categorization of both coarse and fine aggregates of coral reef limestone.

Contrasting with traditional land-based sand and gravel, fragments of reef limestone display features like suboptimal particle form, uneven particle shapes, coarse surfaces, significant porosity, extensive specific surface area, and reduced strength (Luo et al., 2023). Therefore, more cement paste is required to enhance workability when mixing concrete, making it less suitable for high-strength concrete applications. This research involved blending both coarse and fine reef limestone aggregates with standard Portland cement, seawater, fly ash, slag, and various additives, as

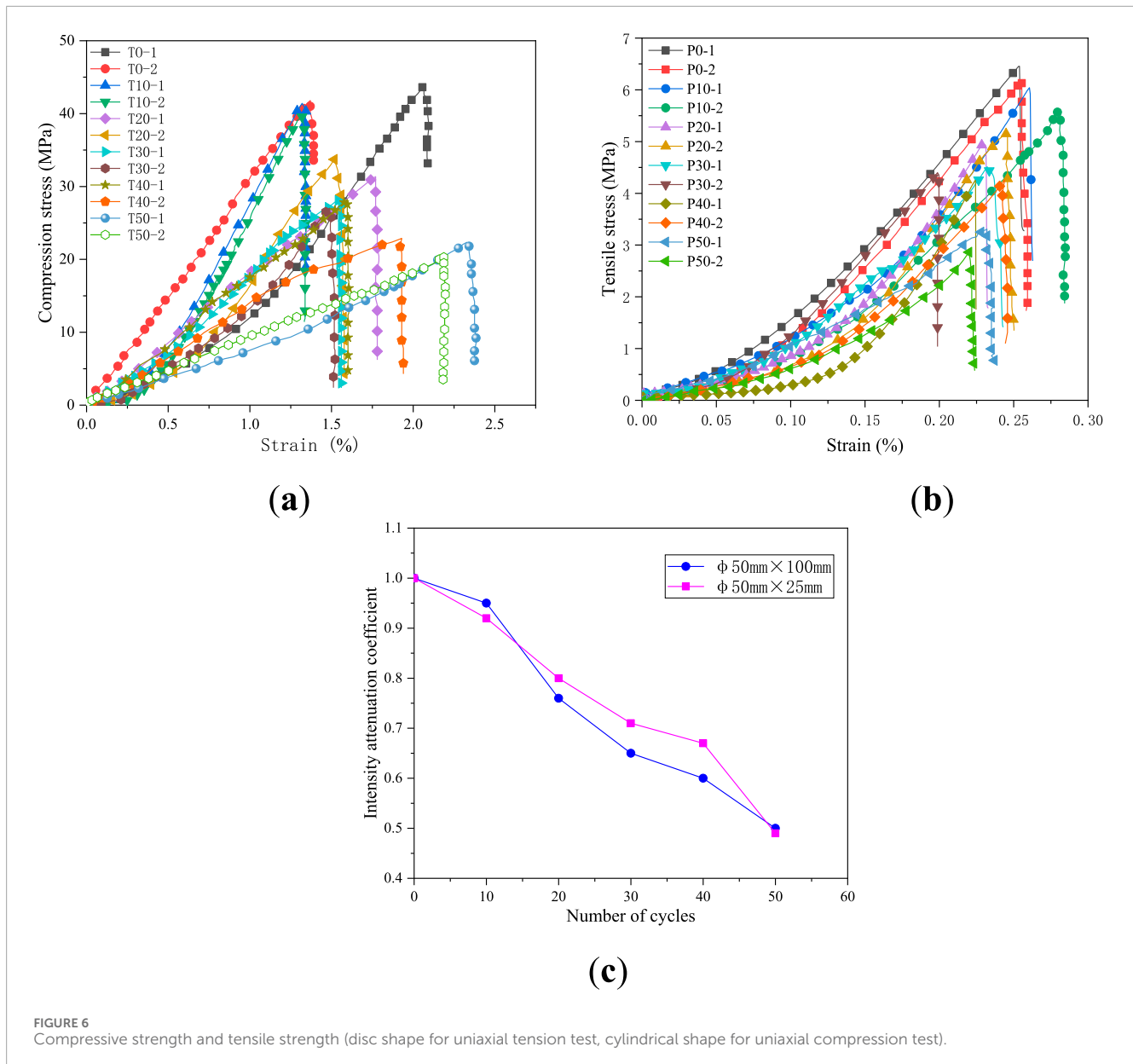


FIGURE 6 Compressive strength and tensile strength (disc shape for uniaxial tension test, cylindrical shape for uniaxial compression test).

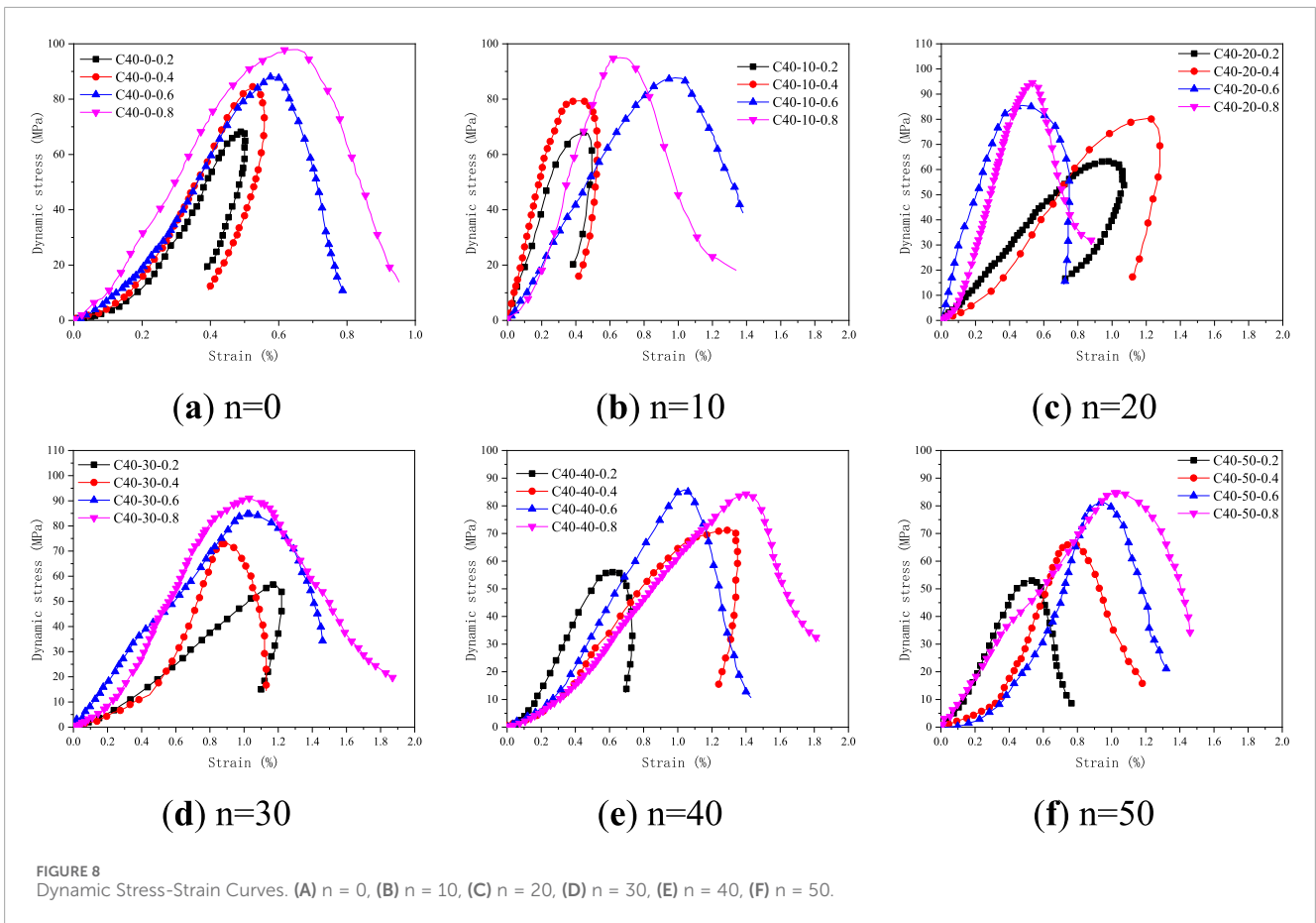
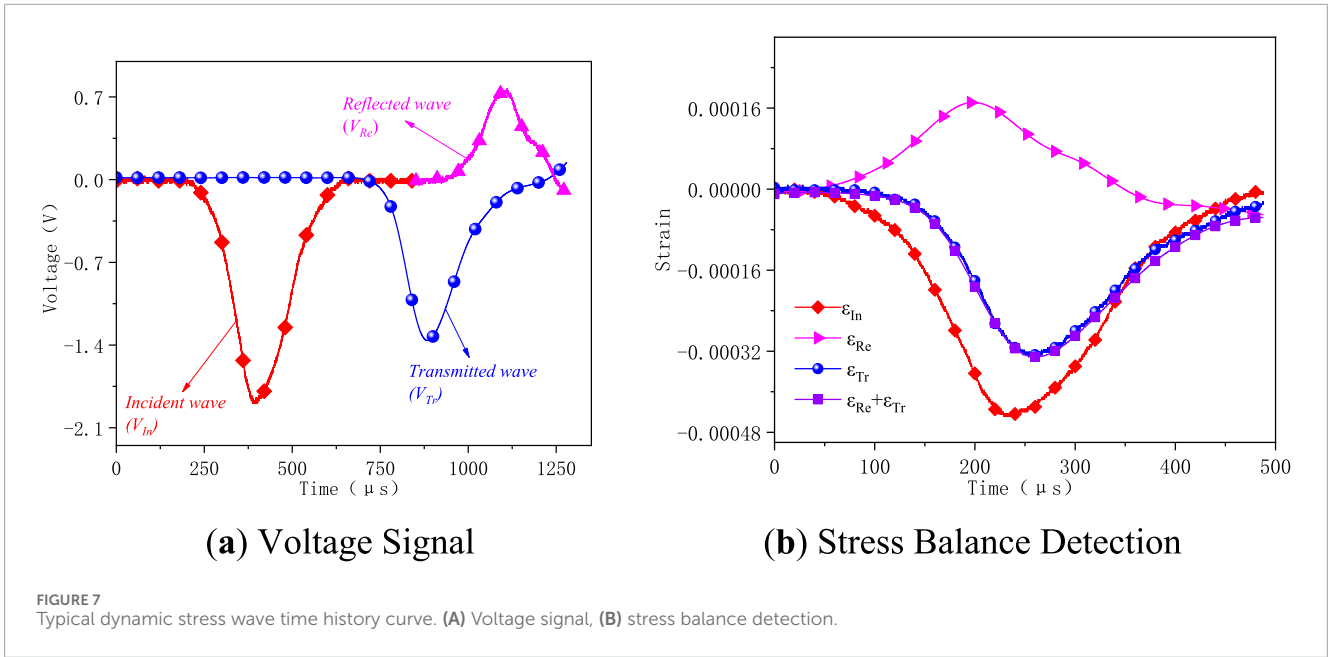
detailed in Table 1, to create concrete with a C40 strength. Notably, the aggregates of reef limestone underwent water immersion before being mixed to eliminate detrimental ions and contaminants. After processes such as mixing, vibrating, and curing, cylindrical specimens with height-to-diameter ratios of 1:2 ($\phi 50\text{ mm} \times 25\text{ mm}$) and 2:1 ($\phi 50\text{ mm} \times 100\text{ mm}$) were prepared.

2.2 Dry-wet carbonation

Figure 2 illustrates the entire process of the dry-wet carbonation cycle that the reef limestone concrete samples underwent. Before the experiments, the samples were subjected to a drying pretreatment (assessed by changes in mass to determine whether they reached a dry state). In order to ensure the rationality of the dry-wet carbonation cycle pretreatment scheme, the existing research results

are referred to Wang et al. (2018); Jiang et al. (2017); Zhang and Shao (2016). First, the dried samples were placed in a vacuum saturation container filled with seawater (soaked in a vacuum state for 12 h). Subsequently, the samples, once saturated, underwent a drying phase in an oven maintained at a steady 60°C for 12 h. Ultimately, the specimens were positioned in a carbonation chamber to undergo carbonation treatment, characterized by a carbon dioxide level of $20\% \pm 3\%$, a humidity of $70\% \pm 5\%$, a temperature maintained at $20^\circ\text{C} \pm 5^\circ\text{C}$, and a 24-h period. The trio of stages forms a single cycle, with the count of dry-wet carbonation cycles adjusted to 0, 10, 20, 30, 40, and 50 cycles.

Micro-fissures in the reef limestone concrete samples will progressively widen and enlarge due to dry-wet carbonation cycles, resulting in the unavoidable seepage of internal elements. Initially, the specimens have relatively high density and stronger resistance to dry-wet cycles and carbonation. However, with the rise in cycle



count, there will be a noticeable alteration in the ultimate weight of the samples. Consequently, the rate at which mass is lost serves as an indicator of the extent of damage and degradation. The method and procedure for calculating the mass loss rate are as follows:

- 1) Dry the specimens after completing the dry-wet carbonation cycles, and wrap them in plastic wrap to prevent moisture from causing errors, then weigh each specimen three times and take the average value as its initial mass; 2) Place the specimens

TABLE 2 Overview of characteristic parameters under impact load.

Number of deterioration cycles	Impact Load/MPa	Strain rate/s-1	Dynamic peak Strength/MPa	Peak strain/%	DIF
0	0.2	54.65	68.20	0.489	1.60
	0.4	83.88	84.48	0.524	1.98
	0.6	106.57	88	0.576	2.06
	0.8	124.60	97.90	0.644	2.29
10	0.2	62.80	68.00	0.45	1.59
	0.4	83.37	79.40	0.42	1.86
	0.6	116.31	87.70	0.98	2.05
	0.8	132.91	95.00	0.66	2.22
20	0.2	66.75	63.25	0.956	1.48
	0.4	90.91	80.34	1.21	1.88
	0.6	111.36	85.50	0.47	2.00
	0.8	144.17	94.5	0.53	2.21
30	0.2	77.16	56.70	1.2	1.33
	0.4	91.63	72.93	0.87	1.71
	0.6	118.66	84.7	1.02	1.98
	0.8	144.56	91.00	1.03	2.13
40	0.2	76.19	56	0.619	1.31
	0.4	94.91	71.17	1.29	1.67
	0.6	129.31	85.80	1.04	2.01
	0.8	150.26	84.24	1.4	1.97
50	0.2	83.3	53.00	0.54	1.24
	0.4	106.17	66.70	0.77	1.56
	0.6	132.32	81.00	0.93	1.90
	0.8	158.33	84.70	1.02	1.98

into the corresponding equipment for the deterioration test according to the experimental protocol, and after undergoing the specified number of deterioration tests, remove the specimens, dry them, and weigh them; 3) Utilize the following formula to determine the rate at which the specimens lost mass following the n th deterioration test. Formula 1 is as follows:

$$\Delta m_n = \frac{m_0 - m_n}{m_0} \times 100\% \quad (1)$$

In the equation, Δm_n represents the mass loss rate of the specimen (%); m_0 denotes the initial mass (g); and m_n represents the mass after undergoing n deterioration actions (g). Furthermore, the E_{rd} relative dynamic modulus of elasticity serves as a crucial measure for evaluating the specimens' damage and degradation. This refers to the proportion between the specimen's dynamic modulus of elasticity post the n th cycle and its initial dynamic modulus of elasticity. To prevent secondary damage during the testing process from causing experimental errors, the elastic modulus is

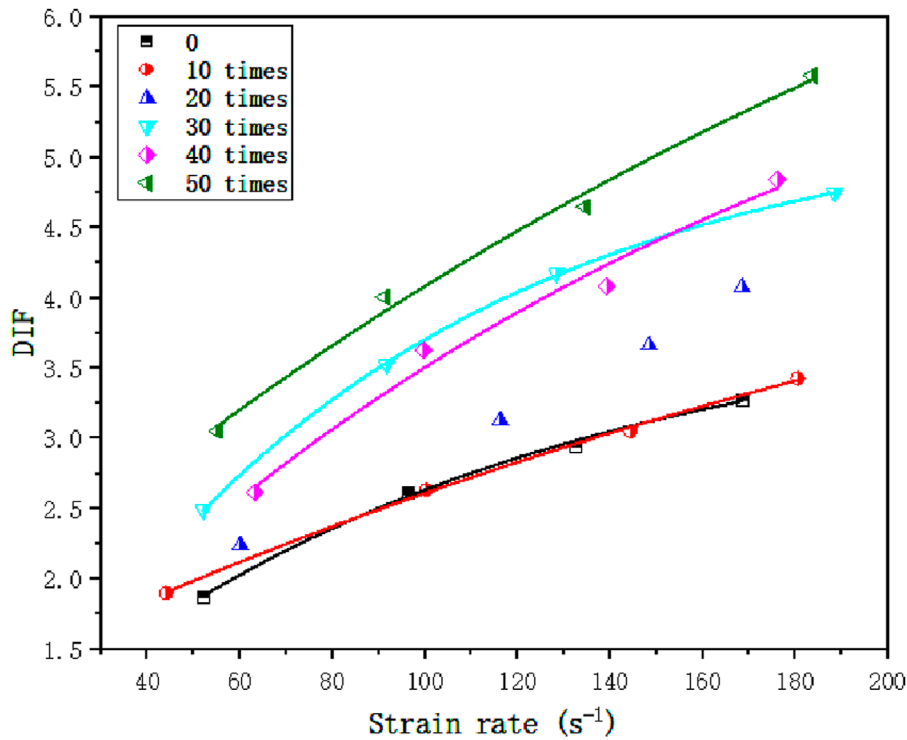


FIGURE 9 The fitting curves of DIF of specimens under different deterioration times.

calculated using parameters such as sound travel time and wave speed while ultrasonic waves propagate through the specimen. This method is completely non-destructive to the specimen, as shown in Equations 2, 3.

$$E_{rd} = \frac{E_{dn}}{E_{d0}} = \frac{V_n^2}{V_0^2} \tag{2}$$

$$E_d = \frac{(1 + \nu)(1 - 2\nu)\rho V^2}{1 - \nu} \tag{3}$$

In the equation, E_d represents the dynamic modulus of elasticity of the specimen (GPa); ν represents the Poisson’s ratio of the specimen; ρ represents the density of the specimen (kg/m^3); V is the ultrasonic wave speed (m/s); E_{d0} is the initial dynamic modulus of elasticity of the specimen (GPa), and E_{dn} is the dynamic modulus of elasticity after undergoing n deterioration actions (GPa).

2.3 Impact testing equipment and testing principles

Using a divided Hopkinson pressure bar, dynamic compression experiments were performed on reef limestone concrete samples that had experienced cycles of dry and wet carbonation. The experimental setup is shown in Figure 3. The incident bar and the transmission bar are both 2,800 mm, the bar diameter is 50 mm, the elastic modulus is 210 GPa, and the density is $7,800 \text{ kg/m}^3$. Introducing high-pressure gas into the emission chamber propels

the projectile at a specific speed, hitting the incident bar’s end surface and creating a longitudinal compressive wave. Upon the arrival of this compressive wave at the specimen, a sequence of transmission and reflection events take place at the terminal surfaces of both the incident and transmission bars. Strain gauges affixed to both the incident and transmission bars record the incident strain ϵ_i , the reflected strain ϵ_r , and the transmitted strain ϵ_t . Ultimately, by presuming one-dimensional stress waves and uniformity, one can determine the specimen’s stress-strain and loading rate data.

























As per the principles of one-dimensional stress wave theory, the stress and strain of the specimen can be determined by the following Formula 4 (Dai et al., 2010):

$$\begin{aligned} \sigma_t &= \frac{(\epsilon_i(t) + \epsilon_r(t) + \epsilon_t(t))E_0A}{2A_s} \\ \dot{\epsilon}(t) &= \frac{(\epsilon_i(t) - \epsilon_r(t) - \epsilon_t(t))C_0}{L_s} \\ \epsilon(t) &= \int_0^t \dot{\epsilon}(t)dt \end{aligned} \tag{4}$$

Within the formula, E_0 , C_0 , and A symbolize the velocity of the elastic wave within the bar, the elastic modulus, and the bar’s cross-sectional area, in that order; A_s and L_s denote the specimen’s cross-sectional area and length, respectively; and t denotes the stress wave’s length.

In addition, the calculation Formula 5 of the incident energy W_I , reflected energy W_R and transmitted energy W_T on the pressure rod during the whole process from the beginning of loading to the failure

TABLE 3 Typical fracture modes of reef limestone concrete under impact load.

Load break Times	0.2 MPa	0.4 MPa	0.6 MPa	0.8 MPa
0				
10				
20				
30				
40				
50				

of the sample is as follows (Huang et al., 2014):

$$\begin{aligned}
 W_I &= \frac{C_0 A}{E_0} \int \sigma_T^2(t) dt, \\
 W_R &= \frac{C_0 A}{E_0} \int \sigma_R^2(t) dt, \\
 W_T &= \frac{C_0 A}{E_0} \int \sigma_T^2(t) dt
 \end{aligned} \quad (5)$$

Given that the energy dissipation of the stress wave in both the bar and the specimen is deemed minimal, the aggregate energy the specimen absorbs and dissipates, denoted as W_L , is derivable from the subsequent Equation 6.

$$W_L = W_I - (W_R + W_T) \quad (6)$$

3 Analysis of experimental results

3.1 Results of static mechanical properties tests

The primary cause of carbonation in reef limestone concrete lies in CO_2 penetrating its core, leading to a decrease in its

alkalinity. Samples subjected to varying degrees of deterioration were cut and sprayed with a 1% phenolphthalein ethanol solution. The color reaction of the phenolphthalein ethanol solution is shown in Figure 4. After different numbers of deterioration cycles, the degree of carbonation represented by the phenolphthalein reagent varied. The undeteriorated samples showed a strong magenta color after treatment with phenolphthalein, while the degree of color change gradually weakened with an increasing number of deterioration cycles.

It is noteworthy that the reef limestone aggregate was also stained by the phenolphthalein reagent. This is because, after the aggregate underwent pre-absorption of water, more cement paste entered its interior during the mixing process, which increased the alkalinity of the aggregate. As the number of deterioration cycles increased, the cement content in the pores of the aggregate gradually decreased, resulting in a gradual reduction in the staining intensity under the phenolphthalein reagent. Further testing showed that the carbonation depth of reef limestone concrete at different deterioration levels increased by 1.5%, 1.58%, 2.87%, and 5.6% compared to the standard condition. Among them, the sample of reef limestone concrete with the deepest deterioration had a carbonation depth increase of 5.2 mm compared to the standard condition. He et al. research shows that cyclic dry-wet carbonation

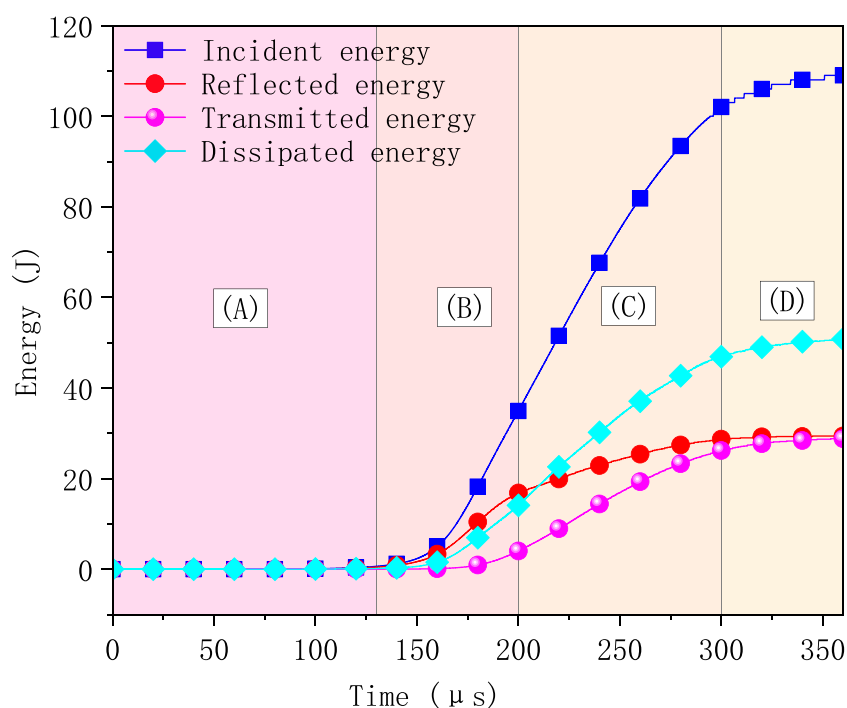


FIGURE 10
Energy-time curve under impact load.

can lead to changes in the pore structure of concrete and cause the reorganization of hydration products, affecting its structural strength. For example, some hydration products (such as C-S-H gel) may convert into lower-strength calcium carbonate, thereby weakening the overall strength and reducing its durability (He et al., 2022).

Figure 5 summarizes the mass loss rates and relative elastic moduli of reef limestone concrete specimens subjected to different numbers of deterioration cycles. When the mass loss rate reaches over 5%, the specimen can be deemed damaged. For cylindrical specimens ($\phi 50 \text{ mm} \times 100 \text{ mm}$), the mass loss rate did not exceed 5% even after more than 40 deterioration cycles, while the disc specimens ($\phi 50 \text{ mm} \times 25 \text{ mm}$) exhibited a high mass loss rate, indicating that the dry-wet carbonation cycles caused significant damage to the disc samples. Overall, although the shapes of the specimens differ, both types experienced an increase in mass loss rates with the growing number of deterioration cycles, although the trends in their growth were distinct. Furthermore, the relative dynamic elastic modulus displayed a significant size effect influenced by the number of dry-wet carbonation cycles. With the ongoing rise in deterioration cycles, there was an acceleration in the decrease rate of the cylindrical specimens' relative dynamic elastic modulus ($\phi 50 \text{ mm} \times 100 \text{ mm}$), as evidenced by the reduced acoustic wave velocity. This suggests a swift escalation and ongoing spread of cracks within the specimens, thereby intensifying their damage severity. Conversely, the disc specimens' dynamic elastic modulus ($\phi 50 \text{ mm} \times 25 \text{ mm}$) varied in tandem with the escalation of deterioration cycles. This difference reflects the varying internal structural responses of different specimens during the deterioration process; the cylindrical

specimens may exhibit better resistance to deterioration due to their structural characteristics compared to other types of specimens.

Furthermore, quasi-static compression and tension tests were conducted on reef limestone concrete samples subjected to varying degrees of deterioration, and the statistical results are shown in Figure 6. Despite variations in the data from uniaxial compression and tension tests, it's noticeable that the specimens' uniaxial compressive and tensile strengths exhibit a general downward trajectory after varying levels of degradation, with a direct relationship between the rise in peak strain and the frequency of these deterioration cycles.

Referring to Deng et al. (2020a); Deng et al. (2020b) research results, the ratio of strength is used as an increasing coefficient. The strength reduction coefficient is defined as the strength reduction coefficient is the ratio of uniaxial compressive strength of the sample after dry-wet carbonation cycle to that of the initial sample, to evaluate the degree of deterioration of reef limestone concrete specimens. When the number of deterioration cycles is less than 20, the strength attenuation is not significant, with the average compressive strength remaining above 40 MPa. However, once the count of degradation cycles surpasses 20, the reduction in strength becomes more noticeable, evidenced by the average compressive strength falling from 32.53 to 25.55 MPa. When samples undergo 40 cycles of decay, their uniaxial compressive strength drops to merely 60% of their original level, and upon reaching 50 cycles, the mean compressive strength drops to just 21.32 MPa. The maximum average tensile strength of the specimens is 6.31 MPa, but after 50 cycles of deterioration, the maximum tensile strength decreases to

TABLE 4 Energy characteristic values of reef limestone concrete under different impact loads and number of deterioration cycles.

Number of deterioration cycles	Impact Load/MPa	Strain Rate/s ⁻¹	Incident Energy/J	Reflected Energy/J	Transmitted Energy/J	Dissipated energy
0	0.2	54.65	80.95	19.21	27.30	34.44
	0.4	83.88	108.11	35.45	36.03	26.63
	0.6	106.57	138.85	48.64	36.21	54.00
	0.8	124.60	171.22	57.67	26.99	86.56
10	0.2	62.80	76.08	15.27	25.69	35.13
	0.4	83.37	106.47	47.80	32.72	15.95
	0.6	116.31	139.61	35.74	45.26	58.61
	0.8	132.91	166.03	59.64	27.6	78.79
20	0.2	66.75	71.39	17.58	22.43	31.37
	0.4	90.91	105.75	42.45	30.39	22.91
	0.6	111.36	133.83	40.46	39.56	53.81
	0.8	144.17	160.69	54.19	27.86	78.64
30	0.2	77.16	72.10	15.47	14.66	41.97
	0.4	91.63	106.26	37.50	31.22	36.54
	0.6	118.66	133.77	37.5	39.89	56.38
	0.8	144.56	170.47	59.68	28.98	81.81
40	0.2	76.19	78.20	16.73	14.45	47.02
	0.4	94.91	106.11	33.63	32.51	29.97
	0.6	129.31	131.26	30.73	35.47	65.06
	0.8	150.26	165.12	57.55	20.01	87.56
50	0.2	83.3	79.36	16.20	12.73	50.42
	0.4	106.17	109.20	29.40	28.82	50.98
	0.6	132.5	132.5	25.39	26.49	80.62
	0.8	158.33	170.95	57.13	24.66	89.16

3.31 MPa, resulting in an overall tensile strength reduction of 49%. The reduction in tensile strength is lower than that of compressive strength.

3.2 Dynamic compression characteristic test results

3.2.1 Dynamic stress balance verification

The dynamic impact tests were conducted on coral reef limestone concrete specimens that had undergone 0, 10, 20, 30, 40,

and 50 cycles of wet-dry carbonation treatment. The impact loads considered were 0.2, 0.4, 0.6, and 0.8 MPa, respectively. As per the ISRM (International Society for Rock Mechanics) guidelines for dynamic analysis of rock-like substances, conducting a preliminary test prior to the official experiment is essential to verify the experiment's accuracy and reduce errors in the process. In the initial testing phase, semiconductor strain gauges were employed to measure three wave signals, and the uniformity of stress in the samples was confirmed through the three-wave technique. A test is deemed legitimate if the stress exerted at either end of the specimen is evenly distributed.

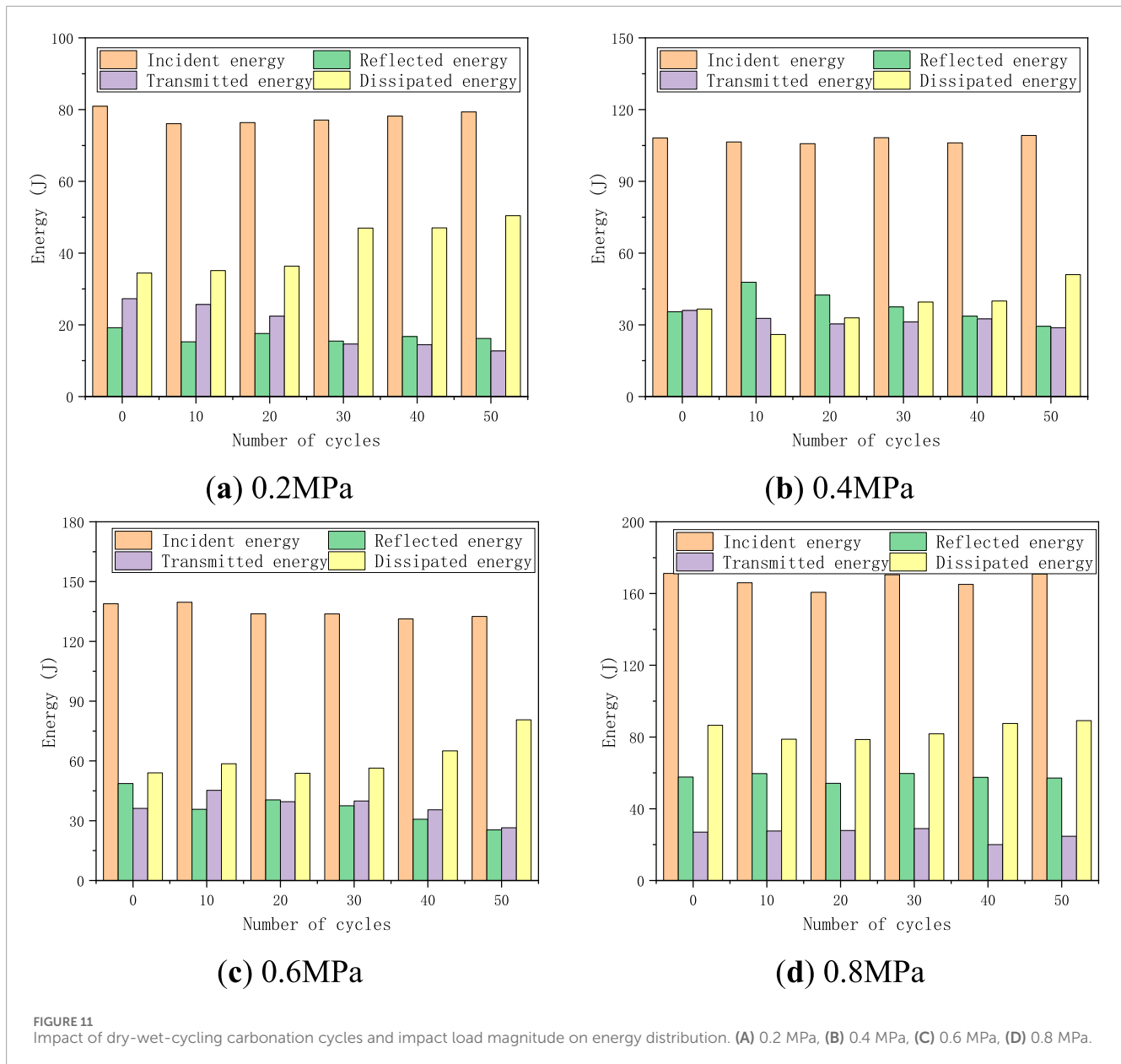


Figure 7A shows the voltage signals of the incident wave, reflected wave, and transmitted wave collected by the strain gauges during a single impact test, Incident Strain $\epsilon_{In(t)}$, Reflected Strain $\epsilon_{Re(t)}$ and Transmitted Strain $\epsilon_{Tr(t)}$. The three-wave method was used for illustration and analysis, as shown in Figure 7B, the incident strain $\epsilon_{In(t)}$ and the reflected strain $\epsilon_{Re(t)}$ roughly coincide with the transmitted strain $\epsilon_{Tr(t)}$ after superposition ($\epsilon_{In(t)} + \epsilon_{Re(t)} \approx \epsilon_{Tr(t)}$). This indicates that dynamic stress uniformity was achieved in the reef limestone concrete sample during the impact loading test.

3.2.2 Dynamic strength and deformation characteristics

Figure 8 depicts the dynamic stress-strain curves of reef limestone concrete under different impact load conditions (after experiencing varying degrees of deterioration treatment). Both the number of deterioration cycles and the magnitude of the impact load

significantly influence the dynamic stress-strain response of the reef limestone concrete. The characteristic parameters of each test result are shown in Table 2. Among these, dynamic compressive strength is an important indicator of the sample's impact resistance. By using the dynamic peak strength and uniaxial compressive strength, another indicator of impact resistance, the Dynamic Increase Factor (DIF), can be calculated.

An examination of Figure 8 and Table 2 reveals that in the condition lacking any degradation treatment ($n = 0$), as the impact load escalates from 0.2 MPa to 0.8 MPa, there's a rise in dynamic peak stress from 68.20 MPa to 88 MPa, with corresponding increases of 23.87%, 29.03%, and 43.5%, in contrast to outcomes not influenced by deterioration. This indicates that the dynamic strength of the material enhances strain rate. Furthermore, with a total of 50 degradation cycles, the maximum dynamic stress at a 0.2 MPa impact load reaches 53 MPa, while impact loads of 0.4, 0.6 MPa, and

0.8 MPa exhibit increases of 25.8%, 52.8%, and 58.49% respectively. This suggests that as the extent of deterioration increases, so does the susceptibility of the specimen's dynamic mechanical characteristics to the rate of strain. However, with the increase in the number of deterioration cycles, the peak stress exhibits a consistent downward trend. As an illustration, at an impact load of 0.2 MPa, following 50 cycles of dry-wet carbonation, the stress-strain curve's post-peak phase shifts from closed to open, experiencing a reduction in peak stress by about 10–20 MPa. It should be noted that due to issues such as uneven crushing of reef limestone aggregate during specimen preparation and uneven composition of aggregate and cementitious materials in the mold, some samples did not maintain good dependency between peak strain, number of deterioration cycles, and impact load under dynamic load conditions.

Perform a nonlinear fitting curve of the strain rate-DIF for reef limestone concrete specimens with different degrees of deterioration. The fitting curve model is $DIF = \ln(a + b\dot{\epsilon})$. The correlation coefficients are all greater than 95%. Figure 9 illustrates that in conditions of elevated strain rates, as the specimen's degradation depth progressively deepens, there's a rising trend in the logarithmic-DIF curve's slope for strain rate, signifying a gradual escalation in the strain rate impact of reef limestone concrete.

3.2.3 Dynamic fracture mode

Table 3 summarizes the fracture conditions of reef limestone concrete under dynamic impact after different degrees of deterioration treatment. The impact load and the number of dry-wet carbonation cycles jointly determine the final failure mode of the specimen. Initially, by maintaining a steady count of dry-wet carbonation cycles, the extent of the specimen's fragmentation is intimately linked to the intensity of the impact load. When the impact load is 0.2 MPa, the surface of the specimen fractures, showing splitting failure with good overall integrity. However, as the impact force escalates to either 0.6 or 0.8 MPa, the sample is utterly obliterated, resulting in tinier fractured particles, predominantly in a powdery state. d particles are smaller, mainly in a powdery form. Additionally, maintaining a steady impact load, there's a positive relationship between the extent of the specimen's fragmentation and the frequency of dry-wet carbonation cycles. When subjected to an impact force of 0.2 MPa, the sample lacking dry-wet carbonation results in minimal surface debris, in contrast to the sample that undergoes 50 cycles of dry-wet carbonation, leading to significant fractures. When the impact load reaches 0.6 MPa, it is visually evident from the size of the fractured particles that the deterioration causes severe internal damage to the specimen, and the pulverization characteristic of the specimen becomes more significant compared to the specimen without dry-wet carbonation treatment.

The reasons for the above phenomenon can be roughly summarized into the following two points. Initially, the dry-wet carbonation cycles lead to the primary presence of free water between the cement mortar and its boundary, consequently diminishing the robustness of the cement matrix and the specimen's interface, thereby increasing the likelihood of dynamic failure, particularly evident in the more pronounced failure rate between these phases. Under the cyclic action of external factors, the internal cracks of concrete will change from micro to macro (Kuang et al., 2023). Secondly, following the combined effects of dry-wet cycles and carbonation, the internal stress of reef limestone concrete

transitions from equilibrium to imbalance under dynamic forces. In a very short period, the specimen cannot achieve internal stress rebalancing through elastic unloading, leading to the absorption of energy by internal cracks, which begin to propagate and eventually cause extensive fracturing of the specimen.

3.2.4 Energy dissipation characteristics

The principal cause of the specimen's malfunction is the loss of energy during its dynamic fracturing. Under impact load, reef limestone concrete experiences irreversible deformation, leading to irreversible energy dissipation. The dimensions, amount, and spatial arrangement of the fragments created post dynamic compression failure represent a large-scale expression of energy loss. Illustrated in Figure 10, the energy-time graph of a reef limestone concrete sample, after undergoing 50 cycles of dry-wet carbonation with a 0.4 MPa impact load, can be broadly segmented into four distinct phases for analysis.

In region A (0–130 μ s), the incident stress wave has not yet acted on the reef limestone concrete specimen. As the incident energy starts to rise, the procedure progresses to stage B (130–200 μ s), during which the specimen's energy absorption curve shows a roughly linear increase. The rate of expansion exceeds that of the energy transmitted and closely mirrors the energy reflected. Throughout the 200–300 μ s phase, there's a consistent linear increase in the absorbed energy timeline, mirroring the pattern of energy transmission and exhibiting a growth rate surpassing that of the reflected energy. The reason is that following the stress wave's impact on the specimen, there's a buildup and development of internal damage, resulting in a multitude of new microcracks in the specimen and a steady rise in the energy absorbed. During the 300–350 μ s phase, there's a steady decline in the rate of energy absorption, with the incoming, reflected, and transmitted energy levels stabilizing, signifying the stress wave's completion of its dynamic compression impact on the sample. The energy characteristic values of reef limestone concrete specimens subjected to different degrees of deterioration under various impact loads are summarized in Table 4.

Figure 11 displays the ratios of incoming, reflected, transmitted, and dissipated energy in reef limestone concrete when subjected to impact forces of 0.2, 0.4, 0.6, and 0.8 MPa. Comprehensive examination reveals that the variance in incident energy from the experiments remains below 5% under an identical impact load, suggesting a uniform impact load across the experiment. With an increasing number of deterioration cycles, the energy dissipated during the fracturing of reef limestone concrete gradually increases, indicating that the dry-wet-carbonation cycling has a promoting effect on dissipated energy. If the count of dry-wet cycling-carbonation cycles surpasses 30, there's a notable increase in the expansion of energy that has dissipated. As an example, with an impact load of 0.2 MPa, there's a 46.39% rise in the amount of energy lost as the deterioration cycles escalate from 0 to 50. Conversely, the transmitted energy shows an overall declining trend with the increase in deterioration cycles. The main reason for this occurrence is the escalated internal harm to reef limestone concrete post-degradation. In the dynamic compression phase, increased energy is used to enlarge various cracks and move debris, causing a rise in energy dissipation and complicating the stress wave's journey through the specimen to the transmission rod, thereby diminishing the energy transmitted. Additionally, the reflected energy does

not show a clear trend, which may be attributed to the inherent discreteness of the specimen itself.

4 Conclusion

The SHPB impact tests explored how dry-wet-cycling carbonation cycles and the extent of impact load influence the dynamic failure traits and energy development in reef limestone concrete, culminating in these key findings:

- (1) With the rise in dry-wet-cycling carbonation cycles, there's a shift in the phenolphthalein color indicator from a strong magenta hue to a slow decline, signifying a steady reduction in the bonding strength of the specimens' internal structure. There is a notable reduction in the relative dynamic elastic modulus, accompanied by a substantial effect of size and a marked acceleration in the rate of mass loss.
- (2) After undergoing dry-wet-cycling treatment, the quasi-static compressive and tensile strengths of reef limestone concrete exhibit an overall decreasing trend, with the reduction in tensile strength being less pronounced than in compressive strength. As dynamic compressive strength diminishes, the frequency of dry-wet-cycling cycles intensifies the vulnerability of the DIF value to strain rates in reef limestone concrete.
- (3) The total count of dry-wet-cycling cycles combined with the intensity of the impact load collectively dictate the ultimate mode of failure for the specimens. Both factors facilitate the failure, transitioning the fracture mode from surface splitting to catastrophic failure, indicating an increase in the fragility of the material's internal structure.

With the rise in dry-wet-cycling cycles, there's a gradual increase in the energy lost during reef limestone concrete fracturing, alongside a general decrease in the energy transmitted, and the reflected energy lacks a distinct pattern.

Data availability statement

The original contributions presented in the study are included in the article/supplementary material, further inquiries can be directed to the corresponding author.

References

- Dai, F., Huang, S., Xia, K. W., and Tan, Z. (2010). Some fundamental issues in dynamic compression and tension tests of rocks using split Hopkinson pressure bar. *Rock. Mech. Rock. Eng.* 43, 657–666. doi:10.1007/s00603-010-0091-8
- Deng, Z. H., Huang, H. Q., Ye, B. L., Wang, H., and Xiang, P. (2020a). Investigation on recycled aggregate concretes exposed to high temperature by biaxial compressive tests. *Constr. Build. Mater.* 244, 118048. doi:10.1016/j.conbuildmat.2020.118048
- Deng, Z. H., Huang, H. Q., Ye, B. L., and Xiang, P. (2020b). Mechanical performance of RAC under true-triaxial compression after high temperatures. *J. Mater. Civ. Eng.* 32 (8), 04020194. doi:10.1061/(ASCE)MT.1943-5533.0003231
- Deng, Z. H., Wu, D., and Wang, Y. M. (2022). Mechanical properties and failure criteria of coral concrete under true triaxial compression. *J. Mater. Sci.* 57, 17622–17636. doi:10.1007/s10853-022-07728-1
- Donnini, J. (2019). Durability of glass FRCM systems: effects of different environments on mechanical properties. *Compos. Part. B-Eng.* 174, 107047. doi:10.1016/j.compositesb.2019.107047
- Fan, R., Gong, H. L., Luo, Y., Zhang, J., and Li, X. (2023). Experimental characterization of dynamic strength and failure behavior of saturated reef limestone concrete under biaxial stress constraint. *Constr. Build. Mater.* 403, 133116. doi:10.1016/j.conbuildmat.2023.133116
- Fu, Q., Bu, M., Su, L., Guo, B., Chen, L., Song, H., et al. (2021). Dynamic triaxial compressive response and failure mechanism of basalt fibre-reinforced coral concrete. *Int. J. Impact. Eng.* 156, 103930. doi:10.1016/j.ijimpeng.2021.103930
- He, R., Li, S., Fu, C., Zhou, K., and Dong, Z. (2022). Influence of cyclic drying-wetting and carbonation on oxygen diffusivity of cementitious materials: interpretation from the perspective of microstructure. *J. Mater. Civil. Eng.* 34 (10), 04022256.

Author contributions

JL: Project administration, Writing–review and editing, Funding acquisition, Supervision. FL: Writing–review and editing, Conceptualization, Resources, Validation, Visualization. MM: Investigation, Software, Writing–review and editing. JZ: Writing–review and editing, Methodology, Project administration, Writing–original draft. RF: Data curation, Resources, Software, Validation, Writing–original draft.

Funding

The author(s) declare that financial support was received for the research, authorship, and/or publication of this article. The research was supported by the Hainan Provincial Joint Project of Sanya Yazhou Bay Science and Technology City (No. 2021JLH0068), the National Natural Science Foundation of China (No. 51979208), and the Natural Science Foundation of Hainan Province (No. 521CXTD444).

Conflict of interest

The authors declare that the research was conducted in the absence of any commercial or financial relationships that could be construed as a potential conflict of interest.

Publisher's note

All claims expressed in this article are solely those of the authors and do not necessarily represent those of their affiliated organizations, or those of the publisher, the editors and the reviewers. Any product that may be evaluated in this article, or claim that may be made by its manufacturer, is not guaranteed or endorsed by the publisher.

- Huang, S., Liu, H., and Xia, K. (2014). A dynamic ball compression test for understanding rock crushing. *Rev. Sci. Instrum.* 85, 123902. doi:10.1063/1.4902836
- Jiang, C., Huang, Q., Gu, X. L., and Zhang, W. (2017). Experimental investigation on carbonation in fatigue-damaged concrete. *Cem. Concr. Res.* 99, 38–52. doi:10.1016/j.cemconres.2017.04.019
- Kuang, Y., Wang, Y., Xiang, P., Tao, L., Wang, K., Fan, F., et al. (2023). Experimental and theoretical study on the fatigue crack propagation in stud shear connectors. *Materials* 16 (2), 701. doi:10.3390/ma16020701
- Lahiri, S. K., Shaw, A., Ramachandra, L. S., and Maity, D. (2022). Fracture in concrete gravity dams under dynamic loading conditions. *Eng. Anal. Bound. Elem.* 143, 591–605. doi:10.1016/j.enganbound.2022.07.008
- Li, Q. M., Li, X. X., Wang, Y. Z., Xie, T., and Zhou, S. (2021). Effects of coarse aggregate content and salt solution concentration on freeze-thaw damage in concrete. *J. Mater. Civ. Eng.* 33, 04021318. doi:10.1061/(ASCE)MT.1943-5533.0003940
- Liu, J. M., Ou, Z. W., Peng, W., Guo, T., Deng, W., and Chen, Y. (2018). Literature review of coral concrete. *Arab. J. Sci. Eng.* 43, 1529–1541. doi:10.1007/s13369-017-2705-x
- Liu, P. F., Liu, J., and Bi, J. (2023). Experimental and theoretical study of dynamic mechanical behavior of concrete subjected to triaxial confining and impact loads. *J. Build. Eng.* 64, 105715. doi:10.1016/j.job.2022.105715
- Luo, Y., Gong, H. L., Wei, X. Q., Zheng, S., Pei, C., and Li, X. (2023). Dynamic compressive characteristics and damage constitutive model of coral reef limestone with different cementation degrees. *Constr. Build. Mater.* 362, 129783. doi:10.1016/j.conbuildmat.2022.129783
- Ma, H., Yue, C., Yu, H., Mei, Q., Chen, L., Zhang, J., et al. (2020). Experimental study and numerical simulation of impact compression mechanical properties of high strength coral aggregate seawater concrete. *Int. J. Impact. Eng.* 137, 103466. doi:10.1016/j.ijimpeng.2019.103466
- Ma, L., Li, Z., Liu, J., Duan, L., and Wu, J. (2019). Mechanical properties of coral concrete subjected to uniaxial dynamic compression. *Constr. Build. Mater.* 199, 244–255. doi:10.1016/j.conbuildmat.2018.12.032
- Meddah, M. S., Zitouni, S., and Belaabes, S. (2010). Effect of content and particle size distribution of coarse aggregate on the compressive strength of concrete. *Constr. Build. Mater.* 24, 505–512. doi:10.1016/j.conbuildmat.2009.10.009
- Mumenya, S. W., Tait, R. B., and Alexander, M. G. (2010). Mechanical behaviour of textile concrete under accelerated ageing conditions. *Cem. Concr. Res.* 32, 580–588. doi:10.1016/j.cemconcomp.2010.07.007
- Qin, Q., Meng, Q., Mei, Q., Wu, K., Wang, C., and Zhang, J. (2023). Dynamic response characteristics of coral reef sand concrete under impact loading. *J. Build. Eng.* 66, 105847. doi:10.1016/j.job.2023.105847
- Sim, J. I., Yang, K. H., and Jeon, J. K. (2013). Influence of aggregate size on the compressive size effect according to different concrete types. *Constr. Build. Mater.* 44, 716–725. doi:10.1016/j.conbuildmat.2013.03.066
- Uddin, M. T., Mahmood, A. H., Kamal, M. R. I., Yashin, S., and Zihan, Z. U. A. (2017). Effects of maximum size of brick aggregate on properties of concrete. *Constr. Build. Mater.* 134, 713–726. doi:10.1016/j.conbuildmat.2016.12.164
- Wang, J., Su, H., and Du, J. (2018). Influence of coupled effects between flexural tensile stress and carbonation time on the carbonation depth of concrete. *Constr. Build. Mater.* 190, 439–451. doi:10.1016/j.conbuildmat.2018.09.117
- Wu, J. W., Ma, L. J., Kong, X. L., Luo, Z. M., and Duan, L. Q. (2020). Dynamic properties of coral concrete under impact load. *J. Build. Mater.* 23, 581–588. (in Chinese). doi:10.3969/j.issn.1007-9629.2020.03.014
- Wu, W. J., Wang, R., Zhu, C. Q., Meng, Q., and Liu, H. (2019). Experimental study on dynamic compression performance of coral aggregate concrete. *J. Build. Mater.* 22, 7–14. (in Chinese). doi:10.3969/j.issn.1007-9629.2019.01.002
- Xu, H., Wang, Z., Shao, Z., Cai, L., Jin, H., Zhang, Z., et al. (2021). Experimental study on durability of fiber reinforced concrete: effect of cellulose fiber, polyvinyl alcohol fiber and polyolefin fiber. *Constr. Build. Mater.* 306, 124867. doi:10.1016/j.conbuildmat.2021.124867
- Yin, S., Jing, L., Yin, M., and Wang, B. (2019). Mechanical properties of textile reinforced concrete under chloride wet-dry and freeze-thaw cycle environments. *Cem. Concr. Res.* 96, 118–127. doi:10.1016/j.cemconcomp.2018.11.020
- Zhang, D., and Shao, Y. (2016). Early age carbonation curing for precast reinforced concretes. *Constr. Build. Mater.* 113, 134–143. doi:10.1016/j.conbuildmat.2016.03.048
- Zhang, M. C., Luo, Y., Gong, H. L., Zhu, Y., and Li, X. (2023). Fine characterization of pore structures in coral reef limestones based on three-dimensional geometrical reconstruction. *Mar. Georesour. Geotec.* 42, 721–735. doi:10.1080/1064119X.2023.2215246
- Zhang, X. B., Quan, Y., Cao, G. H., Tang, S., Ou, W., Cao, J., et al. (2024). Influence of waste glass on concrete strength and permeability during dry-wet cycles. *Eur. J. Environ. Civ. En.*, 1–22. doi:10.1080/19648189.2024.2365960
- Zhou, W., Feng, P., and Lin, H. W. (2020). Constitutive relations of coral aggregate concrete under uniaxial and triaxial compression. *Constr. Build. Mater.* 251, 118957. doi:10.1016/j.conbuildmat.2020.118957